



DE82019549

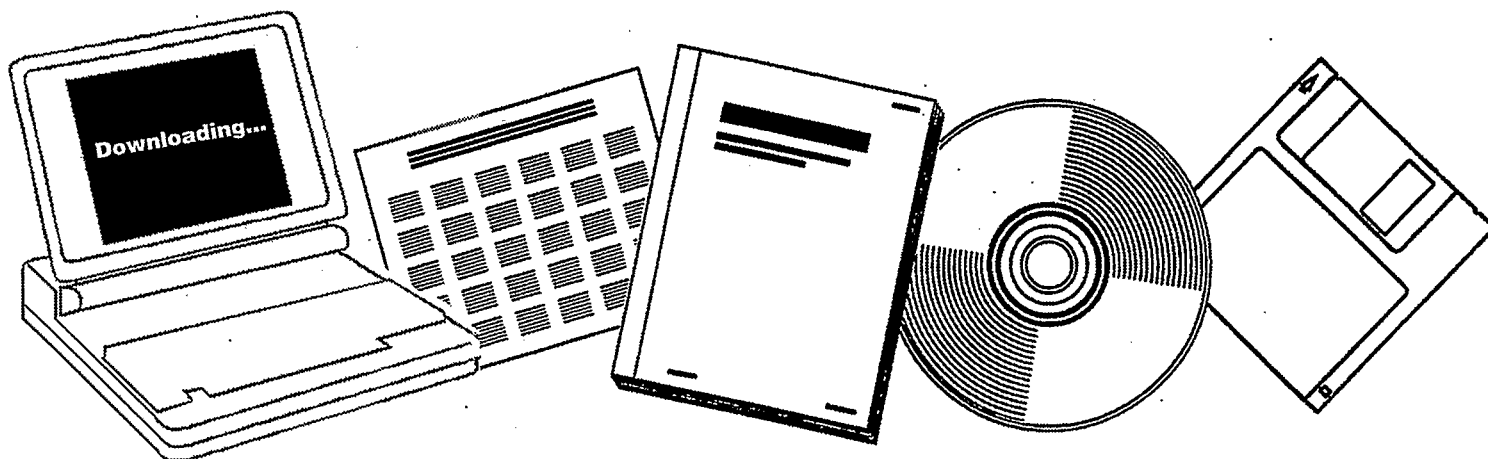
NTIS

One Source. One Search. One Solution.

FISCHER-TROPSCH SYNTHESIS OVER IRON CATALYSTS: THE USE OF REACTIVE SCAVENGERS TO IDENTIFY REACTION INTERMEDIATES

TEXAS UNIV. AT AUSTIN. DEPT. OF CHEMICAL
ENGINEERING

1982



U.S. Department of Commerce
National Technical Information Service



DOE/ER/10720-4
CONF-821706--3

DOE/ER/10720--4

DE82 019549

Fischer-Tropsch Synthesis over Iron
Catalysts: The Use of Reactive Scavengers
to Identify Reaction Intermediates

by

Chia-Zuan Jeff Wang and John G. Ekerdt
Department of Chemical Engineering
University of Texas at Austin
Austin, Texas 78712

MASTER

To be presented at: AIChE Annual Meeting, 1982
Los Angeles; CA

DISCLAIMER

This report was prepared as an account of work sponsored by an agency of the United States Government. Neither the United States Government nor any agency thereof, nor any of their employees, makes any warranty, express or implied, or assumes any legal liability or responsibility for the accuracy, completeness, or usefulness of any information, apparatus, product, or process disclosed, or represents that its use would not infringe privately owned rights. Reference herein to any specific commercial product, process, or service by trade name, trademark, manufacturer, or otherwise, does not necessarily constitute or imply its endorsement, recommendation, or favoring by the United States Government or any agency thereof. The views and opinions of authors expressed herein do not necessarily state or reflect those of the United States Government or any agency thereof.

ABSTRACT

The synthesis of hydrocarbons from H_2 and CO was studied on a silica-supported iron catalyst. The synthesis was carried out at 1.54 atmospheres and 200 to 255°C in a differential reactor. The working catalyst is realized by transforming Fe_2O_3 into a mixture of bulk carbides and iron under synthesis conditions. After the catalyst achieves a steady state condition pulses of a helium stream saturated with pyridine are injected into the reactant gas mixture. The reactor effluent is found to contain alkylpyridines. These are argued to result from pyridine reacting with the alkyl fragments which are formed on the catalyst surface from H_2 and CO. The distribution of alkylpyridines is related to the synthesis product distribution as a means of gaining insight into the synthesis mechanism.

INTRODUCTION

Fischer-Tropsch synthesis of hydrocarbons has received increased attention in recent years. As an understanding of the synthesis phenomena developed, research in the general area has shifted from methane and light hydrocarbon synthesis over simple catalyst systems to higher molecular weight hydrocarbon and oxygenated hydrocarbon synthesis over complex catalysts. Iron represents a complex system capable of generating hydrocarbons over a wide range of molecular weights and varying composition.

Investigations over iron-based catalysts have shown that the chemical composition of the iron phase generally changes during the Fischer-Tropsch reaction (1-10,12,13). Iron is observed to form a mixture of oxides, bulk carbides and an inactive carbon overlayer. The composition is the result of the oxidation-reduction reactions among Fe_3O_4 , Fe, and the carbides and depends upon the temperature, H_2/CO ratio, extent of CO conversion and the duration of the reaction. The fact that an overlayer forms in addition to carbides suggests that CO dissociates and that the resulting carbon reacts with hydrogen to the Fischer-Tropsch products, "graphitizes" into an inactive overlayer or interacts with the bulk metal to form bulk carbides.

The manner in which the carbon interacts with hydrogen is actively being investigated in numerous research laboratories. The synthesis of hydrocarbons over iron-based catalysts have been shown (14,15) to satisfy Schultz-Flory plots. (A linear relation between the log of the mole fraction of product C_n and the carbon

number, n.) Schultz-Flory plots indicate that the synthesis is a stepwise process. The stepwise process probably involves methylene insertion into a growing alkyl chain (16-18). The chain growth process is proposed to describe hydrocarbon synthesis over a variety of metals, including iron.

Alkyl fragments are central to the synthesis mechanism. They can undergo addition of methylene to the next higher alkyl fragment or terminate to an alkane, olefin, or alcohol (19). An understanding of alkyl fragment reactivity and the factors which control alkyl fragment distributions on the catalyst surface will help to elucidate the causes for reaction selectivity and develop improved catalysts.

This paper describes the application of reactive scavenging of hydrocarbon fragments over iron. The technique involves injecting a probe molecule into the reacting mixture and alkylating it with hydrocarbon fragments present on the catalyst surface. Fragments of varying carbon number, probably alkyl fragments, alkylate the probe to give a distribution of substituted probe molecules. The distribution of scavenged fragments is dependent upon synthesis conditions. Scavenging promises to provide an indirect means to measure the effect of synthesis conditions on the surface species participating in the propagation reaction.

The use of scavengers to chemically remove surface intermediates during Fischer-Tropsch synthesis is based upon the organometallic literature. Alkyl (20) and alkylidene ligands (21-23) of metal complexes are reported to undergo elimination

reactions with olefins. Chemical scavengers, olefins, have been used over Ru-based catalysts (24,25). The results have been interpreted to support a methylene insertion process.

Pyridine is selected as the probe molecule because it and any alkylpyridines contain nitrogen, are easily identified with mass spectroscopy and can not be synthesized from H_2 and CO. Other probe candidates such as cyclic or highly branched olefins are produced to varying extents over iron (13). The mechanism by which pyridine is alkylated over iron is not known but can possibly be inferred from studies over nickel. Formation of 2-methylpyridine from methanol (26,27) or H_2/CO (26) over nickel was postulated to proceed via methyl addition to the α -carbon of pyridine. Reinecke and Kray (27) proposed that pyridine bonds to a nickel surface through the nitrogen. The methyl groups were formed by methanol dehydration and decarbonylation and/or the interaction of adsorbed hydrogen and carbon monoxide (27). Methyl and higher alkyl fragments, which are expected over iron, may interact with pyridine adsorbed on iron in a similar fashion to generate α -alkylpyridines.

EXPERIMENTAL

The apparatus, shown schematically in Figure 1, and the experimental techniques are described in more detail elsewhere (13). The reactor is a 6.35 cm section of 0.64 cm OD stainless steel tubing with Swagelok reducing unions on both ends. The catalyst powder is pressed into wafers approximately 0.076 mm thick which are crumbled before placing in the reactor. Less than 0.5 grams is charged to the reactor and carbon monoxide conversion never exceeded 2% at the conditions employed.

The supported iron catalyst was prepared by the incipient wetness technique using 2.0 ml of solution, $\text{Fe}(\text{NO}_3)_3 \cdot 9\text{H}_2\text{O}$ in distilled water, per gram of silica, Cab-O-Sil HS-5. The impregnated support was vacuum dried at 60°C for 42 hours and calcined with breathing air at 300°C for one hour, followed by 20 hours at 400°C. The resulting catalyst contained 20.44 wt % Fe_2O_3 .

The total pressure was maintained constant at 1.54 atmospheres (1 atmosphere equals 101.3 kPa). Temperature was varied between 200 and 250°C. The total volumetric flow rate of reactants ranged from 100 to 110 sccm, resulting in an empty reactor space time of 0.77 to 0.85 seconds.

The fresh catalyst, $\text{Fe}_2\text{O}_3/\text{SiO}_2$, was activated under 4/1 H_2/CO at 230°C for six days prior to attempting any scavenging. The activated catalyst was always exposed to hydrogen and carbon monoxide between 200 and 250°C to maintain the active form. The catalyst was allowed to adjust to a new set of synthesis conditions for at least twelve hours before data were collected.

A helium stream was sparged through the scavenger at room temperature, 0°C or -10°C and vented through an 80 μ l loop on a six-port sample valve. A pulse of the scavenger was added to the reactor feed gas by actuating the valve. Ninety pulses were added at 30 second intervals. The reactor effluent was trapped at liquid nitrogen temperatures for 20 seconds following each injection.

The trap is a 50 ml pear shaped boiling flask. The collected samples were stored in the flask at -10°C for analysis at a later time. Samples were never stored for more than 48 hours.

Trapped products were analyzed on a Varian 3760 GC using a 30 meter x 0.25 mm ID amine deactivated fused silica capillary column loaded with carbowax. Hydrogen was used as the carrier gas and the column was operated at 80°C. The products were washed from the sides of the collection flask with 0.05 ml of diethyl-ether. A splitless Grob-type injector was used and 1.0 to 4.0 μ l was injected.

A background sample was collected along with each scavenged sample. The two were analyzed on the GC and compared to establish the appearance of additional peaks in the chromatogram of the scavenged sample. Relative retention times of the additional peaks are compared against standard mixtures of selected hydrocarbons and alkylpyridines. Occasionally a dilute solution of an alkylpyridine was added to the scavenged sample to help identify a peak. Attempts to confirm elution characteristics and peak identities with a GC-MS met with limited success. Helium had to

be used as the carrier gas on the GC-MS. Carrier flow rate and column temperature could not be optimized to produce the same peak resolution realized with hydrogen on the GC. The GC-MS analysis established that alkylpyridines were eluting and the relative elution order of the alkylpyridines and hydrocarbons. Only the quality of the computer generated assignment for propylpyridine was unsatisfactory because of poor peak resolution.

Fischer-Tropsch products ranging from C_1 to C_6 were also analyzed on the Varian GC. Chromosorb 106 was used for C_1 through C_3 hydrocarbons. An OV-101 column was used for C_4 through C_6 hydrocarbons.

RESULTS AND DISCUSSION

Fischer-Tropsch Characteristics of Iron

It is well established that Fe or Fe_3O_4 will convert into one or more carbide phase under synthesis conditions (1,2,4-10,12,28, 29). The rates at which the phases convert and the changes in synthesis activity and selectivity upon phase change are also reported. Uncertainty in iron phase composition can complicate analysis of data. In an attempt to minimize the uncertainty, the catalyst used in this study, 20.44 wt % $\text{Fe}_2\text{O}_3/\text{SiO}_2$, was conditioned under H_2/CO for six days prior to use and was never exposed to temperatures in excess of 250°C.

Time dependent methanation activity and low weight product selectivity are presented in Figures 2 to 4. These figures display Fischer-Tropsch data over a 40 day period at a common temperature of 230°C. The H_2/CO ratio and partial pressure of CO vary between 3.8 to 4.3 and 0.20 to 0.23 atmospheres, respectively. Some of the scatter of the data may be due to the slight random variation in reactant partial pressure. During this 40 day period the catalyst was also exposed to other pressures and temperatures.

Figure 2 demonstrates the effect the induction period has on methanation activity. After approximately 150 hours the activity reaches a steady value. Activity decreases slightly after 400 to 500 hours.

Figure 3 shows that the distribution of total C_2 to C_5 hydrocarbons (alkanes, olefins, normal and branched) does not change appreciably during the induction period. Only the C_2 's increase

relative to methane during the first 150 hours. These results are presented relative to methane indicating that the selectivity to low weight hydrocarbons is not related to total activity, all hydrocarbons studied, C_1 to C_5 , increase in activity at approximately the same rate. In a separate study (13) it was established that hydrocarbons up to C_{12} , the upper limit investigated, are produced after four hours of reaction.

While the selectivity to C_3 to C_5 hydrocarbons is constant relative to methane during the induction period, the olefin to alkane ratio is not. Figure 4 presents the α -olefin to n-alkane ratio for small hydrocarbons. There is an initial decrease in the olefin to paraffin ratio during early carburization, consistent with other iron-based studies (1,5,6). The olefin to paraffin selectivity returns to the initial selectivity after approximately 120 to 140 hours on stream. The olefins continue to increase slowly over the course of the period studied, whereas the total amount at a particular carbon number is constant.

The activity and product distribution trends shown in Figures 2 to 4 suggest that the Fe_2O_3/SiO_2 is undergoing a rapid transformation into a different active phase during the first 150 hours. This is followed by a slow transformation or deactivation over the remaining 700 hours. The conversion of supported (13) and unsupported Fe_2O_3 (12) into a mixture of carbide phases is reported. Other researchers report the transformation of Fe_3O_4 and Fe into carbide phases (6,30). Reymond et al. (12) relate activity loss to inactive surface carbon formation.

Catalyst used in a different series of experiments but activated in a similar manner and exposed to similar conditions was subjected to X-ray diffraction analysis after 56 days on stream. The diffraction pattern and detailed discussion of peak assignment have been presented elsewhere (13). The patterns are shown in Figure 5. The fresh catalyst charged to the reactor, pattern A, is identified as $\alpha\text{-Fe}_2\text{O}_3$ with an average particle size of 240 Å. The used catalyst, pattern E, displays a broad peak centered at 2θ equal to 43.5° suggesting the presence of several carbide phases. The broad shape displayed by the used catalyst brackets the primary diffraction peaks for $\epsilon\text{-}$, $\epsilon\text{-}$ and $\chi\text{-}$ carbide. These along with $\theta\text{-}$ carbide are known to form from iron under synthesis conditions (10). The broad peak has a shoulder at the location for $\alpha\text{-Fe}$ suggesting that $\alpha\text{-Fe}$ may also be present. Peaks indicating the presence of Fe_2O_3 , Fe_3O_4 , FeO are not detected. Particle size for the used catalyst can not be determined because the peak is poorly resolved.

X-ray diffraction demonstrates that the working catalyst consists of a mixture of bulk carbide phases and possibly some iron. The surface composition is not revealed by the X-ray techniques employed. The bulk phase composition was not characterized immediately after induction, however the slow changes in activity and selectivity suggest that the bulk is not appreciably altered after induction. The slight loss of activity and change to a more olefinic product may result from the growth of an inactive surface carbon layer.

Methanation activity and low weight hydrocarbon selectivity trends can be seen by examining Figures 6 and 7. Figure 6 demonstrates that methanation activity and selectivity to lower molecular weights increase with increasing H_2/CO ratio at a constant temperature. Increasing the temperature at a constant H_2/CO ratio has the same effect upon methanation activity and low weight selectivity. These observations are consistent with other work over iron at 10 atmospheres (14). Figure 7 demonstrates that the major product is the primary olefin. As the H_2/CO ratio increases at constant temperature and CO partial pressure the product becomes more saturated. Increasing the temperature at constant reactant partial pressures appears to increase the olefinic nature of the product. The activity and selectivity trends suggest that as the ability to hydrogenate increases activity and lower weight selectivity increase.

Figure 6 also presents the effect of the synthesis conditions on methanol production. The methanol signal intensity is presented because the GC calibration standards did not contain methanol. Several observations can be made if the sensitivity factor for methanol was constant over the data collection period. As the temperature or H_2/CO ratio is increased the production rate of methanol relative to methane decreases. In addition, as the H_2/CO ratio increases the production rate of methanol increases. The significance of the trends awaits further experimentation.

Scavenging Experiments

Figures 8 and 9 represent the gas-chromatograms for two

different scavenged and background samples. The background products, chromatogram A, are collected in the presence of H_2/CO . The scavenged products, chromatogram B, are collected in the presence of H_2/CO and pyridine. Attention must be paid to the attenuation factors when comparing peaks.

Four additional peaks are seen in the scavenged sample in Figure 8. These peaks correspond to pyridine, 2-picoline (2-methylpyridine), 2-ethylpyridine and 2-propylpyridine. Some of these compounds elute at or near the same time as hydrocarbon compounds. The relative intensity of the suspected alkylpyridine peaks with respect to known hydrocarbon peaks indicates additional compounds are present. The concentration of substituted alkylpyridines is seen to decrease with increasing carbon number.

Figure 9 is qualitatively similar to Figure 8. The concentration of alkylpyridines decreases with increasing carbon number. At the conditions listed in Figure 9 the signal intensity for propylpyridine, peak 18, is only slightly larger than what appears to be a similar peak in the background. Peaks 14, 15, 16, 17, 18 and 19 are not as well resolved on the GC-MS generated chromatograms and can not be conclusively identified. For the scavenged sample the mass fracturing pattern of a compound eluting in the peak 17 to 19 set is clearly associated with a pyridine ring strongly supporting the assignment of propylpyridine.

The signal intensity ratios for the alkylpyridines at a variety of conditions are presented in Table 1. The effect of the pyridine saturation temperature upon the scavenged distribution

was not revealed in the current study, therefore comparisons should only be made at a constant saturation temperature. At all the conditions tested the concentration of substituted pyridines decreases with increasing carbon number.

Methylpyridine to pyridine ratios parallel methane activity dependence upon the synthesis conditions. The first five entries of Table 1, experiments 1 to 5, are at the same conditions represented in Figures 6 and 7. For saturation temperatures of 25°C, methylpyridine yield increases as the H_2/CO ratio or reaction temperature increase. The increase seen at 0°C saturation temperature upon going from 4 to 2 H_2/CO is probably due to the increased H_2 and CO partial pressures at H_2/CO equal to 2. Over 15 wt % Fe/Al_2O_3 the methanation power law rate expression is 1.14 order in H_2 and -0.05 order in CO partial pressure (31). The orders may be different over the catalyst employed here. Assuming the catalyst used in the present study is similar to the group VIII metals, the order can be expected to be near unity for H_2 and near zero for CO (31). Methane activity was not recorded during experiments 6 and 7. It is reasonable to anticipate that methanation activity would increase, therefore the results of experiments 6 and 7 are consistent.

Ethylpyridine to methylpyridine ratios do not correlate completely with the selectivity trends noted earlier. From Figure 6 it can be seen that as the H_2/CO ratio increases the proportion of C_2 's decreases. No trend is displayed in experiments 1 through 3. Increasing the temperature leads to an increase in the C_2 's

but a decrease in the C_3 's, C_4 's and C_5 's. Ethylpyridines increase with temperature.

Propylpyridine to methylpyridine ratios do correspond to the Fischer-Tropsch selectivity trends for the C_3 's. The ratio of C_3/C_1 pyridines decrease with increasing H_2/CO ratio and with decreasing temperature. Too few experiments were performed to address the effect of simultaneously increasing the reactant partial pressures.

Lowering the pyridine saturation temperature and in turn the concentration of pyridine injected produced results which can not be explained at the present time. The methyl yield decreased and the propyl yield increased dramatically. Further experimentation is required to determine the effect of scavenger concentration upon scavenged yield.

Perturbation of the Fischer-Tropsch reaction by the addition of pyridine can be seen by examining Figure 10. The effect on the C_2 to C_5 distribution is similar to that seen over ruthenium. Baker and Bell (32) report that the C_n/C_1 ratio decreases in the presence of olefin scavengers. The decrease is not appreciable until C_7 to C_8 and is almost identical to that seen over iron for C_2 to C_5 when cis-2-butene was used. The decrease at large C_n is expected if the scavenger intercepts a species participating in chain growth. The decrease was not observed in this study because data was not collected in the range C_7 and above.

The olefin to paraffin ratio increases for all carbon numbers in the presence of pyridine. It is unlikely that hydrogen is

reacting with the unsaturated pyridine bonds because pyridine is difficult to hydrocrack between 200 and 250°C (33). A more likely explanation may be that pyridine displaces adsorbed hydrogen, thereby reducing the hydrogenation ability of the catalyst.

Methyl fragments react with pyridine over nickel to produce α -methylpyridine, 2-picoline. All the alkylpyridines detected in this study were α -alkylpyridines suggesting that alkyl fragments were scavenged from the surface of the working catalyst. Methanol was observed as a Fischer-Tropsch product. A series of experiments were performed (13) which eliminate the possibility that alcohols are leading to alkylpyridines over iron at the conditions of this study.

Further support for alkyl fragment scavenging comes from the correlation between alkylpyridine distributions and Fischer-Tropsch selectivity. In the probable Fischer-Tropsch mechanism methyl and methylene fragments are formed by hydrogenating dissociated carbon monoxide. The methyl fragments can undergo hydrogenation to methane or propagation with methylene to generate an ethyl fragment. The ethyl fragment can hydrogenate to ethane, eliminate a hydride to ethylene, or undergo propagation with methylene to generate the propyl fragment. The alkyl fragments are direct precursors to hydrocarbon products and should establish a surface distribution which is similar to the product distribution.

The interpretations presented here are based upon the assumption that alkyl fragment reactivity toward pyridine is independent of the carbon number. This assumption can be tested by examining

the rate of alkylpyridine formation. Experiments are in progress which are attempting to determine the kinetic parameters for alkylpyridine formation. Relationships between alkylpyridine kinetics and Fischer-Tropsch kinetics should provide quantitative insight into the propagation reaction.

CONCLUSIONS

The studies over 20 wt % $\text{Fe}_2\text{O}_3/\text{SiO}_2$ have shown that the iron phase converts into the same type of iron phases seen by other groups starting with Fe_3O_4 and Fe. The bulk phase is identified as a mixture of carbides and possibly some $\alpha\text{-Fe}$. As long as the catalyst is not operated above 250°C the activity remains constant for approximately 700-800 hours.

Alkylpyridines are formed when pyridine is injected into the reactant gas. The alkylpyridine distribution dependence upon synthesis conditions is similar to the dependence displayed by low weight hydrocarbon products. These similarities support a mechanistic description for Fischer-Tropsch synthesis in which alkyl fragments are involved in the surface propagation step.

ACKNOWLEDGMENT

This work was supported by the Division of Chemical Sciences, Office of Basic Energy Sciences, U. S. Department of Energy under Contract DE-AS05-80ER1072.

REFERENCES

1. Ott, G.L., Fleisch, T., and Delgass, W.N., *J. Catal.* 65, 253(1980).
2. Krebs, H.J., Bonzel, H.P., Schwarting, W., and Gafner, G., *J. Catal.* 72, 199 (1981).
3. Dwyer, D.J., and Somorjai, G.A., *J. Catal.* 52, 291 (1978).
4. Raup, G.B., and Delgass, W.N., *J. Catal.* 58, 348 (1979).
5. Raup, G.B., and Delgass, W.N., *J. Catal.* 58, 361 (1979).
6. Amelse, J.A., Butt, J.B., and Schwartz, L.H., *J. Phys. Chem.* 82, 558 (1978).
7. Stanfield, R.M., and Delgass, W.N., *J. Catal.* 72, 37 (1981).
8. Unmuth, E.G., Schwartz, L.H., and Butt, J.B., *J. Catal.* 63, 404 (1980).
9. Amelse, J.A., Schwartz, L.H., and Butt, J.B., *J. Catal.* 72, 95 (1981).
10. Niemantsverdriet, J.W., van der Kraan, A.M., van Dijk, W.L., and van der Baan, H.S., *J. Phys. Chem.* 84, 3363 (1980).
11. King, D.L., *J. Catal.* 61, 77 (1980).
12. Reymond, J.P., Mériaudeau, P., and Teichner, S.J., *J. Catal.* 75, 39 (1982).
13. Wang, C.-Z.J., and Ekerdt, J.G., "Study of Fischer-Tropsch Synthesis over Fe/SiO₂: Reactive Scavenging with Pyridine and Cyclohexene", *J. Catal.* (submitted for publication).
14. Madon, R.J., and Taylor, W.F., *J. Catal.* 69, 32 (1981).
15. Satterfield, C.N., and Huff, G.A., Jr., *J. Catal.* 73, 187 (1982).
16. Brady, R.C., and Pettit, R., *J. Amer. Chem. Soc.* 103, 1287 (1981).
17. Brady, R.C., and Pettit, R., *J. Amer. Chem. Soc.* 102, 6181 (1980).
18. Osterloh, W.T., Cornell, M.E., and Pettit, R., "On the Mechanism of Hydrogenolysis of Linear Hydrocarbons and its Relationship to the Fischer-Tropsch Reaction", *J. Amer. Chem. Soc.* (submitted for publication).

19. Bell, A.T., Catal. Rev. Sci. and Eng. 23, 203 (1981).
20. Evitt, E.R., and Bergman, R.G., J. Amer. Chem. Soc. 101, 3973 (1979).
21. Fellman, J.D., Rupprecht, G.A., Wood, C.D., and Schrock, R.R., J. Amer. Chem. Soc. 100, 5962 (1978).
22. Stevens, A.E., and Beauchamp, J.L., J. Amer. Chem. Soc. 100, 2584 (1978).
23. Grubbs, R.H., and Miyashita, A., J. Amer. Chem. Soc. 100, 7418 (1978).
24. Ekerdt, J.G., and Bell, A.T., J. Catal. 62, 19 (1980).
25. Bell, A.T., "Studies of the Mechanism and Kinetics of Fischer-Tropsch Synthesis over Ruthenium Catalysts" paper 9d AIChE Annual Meeting, November (1981).
26. Myerly, R.C., and Weinberg, K.G., J. Organ. Chem. 31, 2008 (1966).
27. Reinecke, M.G., and Kray, L.R., J. Amer. Chem. Soc. 86, 5355 (1964).
28. Niemantsverdriet, J.W., and van der Kraan, J. Catal. 72, 385 (1981).
29. Shultz, J.F., Hall, W.K., Seligman, B. and Anderson, R.B., J. Amer. Chem. Soc. 77, 213 (1955).
30. Unmuth, E.E., Schwartz, L.H., and Butt, J.B., J. Catal. 61, 242 (1980).
31. Vannice, M.A., J. Catal. 37, 449 (1975).
32. Baker, J.A., and Bell, A.T., "Hydrogenation of Carbon Monoxide Over Ruthenium: Detection of Surface Species by Reactive Scavenging", J. Catal. (submitted for publication).
33. Satterfield, C.N., and Cocchetto, J.F., A.I.Ch.E. J. 21, 1107 (1975).

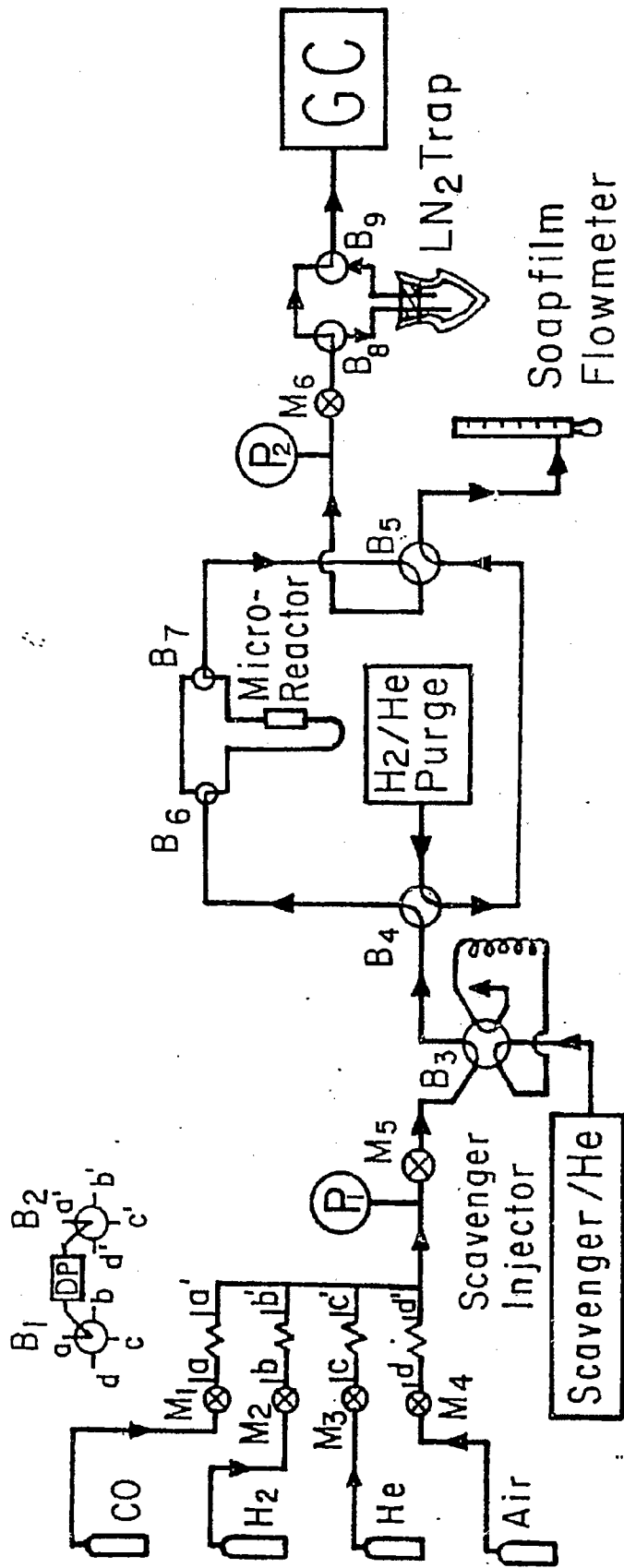
TABLE 1
Effect of the Reaction Conditions
on the Distribution of Alkylpyridines

Experiment	T _{reactor} (°C)	H ₂ /CO	P _{CO} (atm)	T _{pyridine} (°C)	$\frac{C_1\text{-pyr}^{(a)}}{\text{pyr}}$ ($\times 10^1$)	$\frac{C_2\text{-pyr}}{C_1\text{-pyr}}$	$\frac{C_3\text{-pyr}}{C_1\text{-pyr}}$	$\frac{C_3\text{-pyr}}{C_2\text{-pyr}}$
						($\times 10^2$)	($\times 10^3$)	($\times 10^1$)
1	230	2	0.22	25	1.04	2.98	4.00	1.34
2	230	4	0.22	25	3.09	3.87	3.69	0.95
3	230	6	0.22	25	3.05	3.09	2.70	0.87
4	220	2	0.51	25	1.15	3.17	6.00	1.89
5	200	2	0.51	25	0.26	2.76	28.84	10.45
6	242	2	0.51	0	10.76	2.97	8.82	2.97
7	242	4	0.22	0	8.28	3.07	5.89	1.92
8	246	4	0.22	-10	5.87	3.29	10.90	3.31

(a) methylpyridine/pyridine signal intensity ratio

LIST OF FIGURES

- Figure 1. System Schematic
- Figure 2. Rate of methane formation as a function of time on stream.
- Figure 3. Fischer-Tropsch synthesis selectivity to low weight hydrocarbons as a function of time on stream.
- Figure 4. Primary olefin to normal alkane selectivity as a function of time on stream.
- Figure 5. X-ray diffraction patterns, where (a) is 20 wt % $\text{Fe}_2\text{O}_3/\text{SiO}_2$, (b) polyethylene film, (c) partially reduced 10 wt % $\text{Fe}_2\text{O}_3/\text{SiO}_2$, (d) fully reduced 20 wt % $\text{Fe}_2\text{O}_3/\text{SiO}_2$, and (e) catalyst after 56 days of use.
- Figure 6. Product distribution dependence of the low weight synthesis products on the synthesis conditions.
- Figure 7. Primary olefin to normal alkane dependence on the synthesis conditions.
- Figure 8. Chromatogram of the background (curve a) and scavenged products (curve b).
- Figure 9. Chromatogram of the background (curve a) and scavenged products (curve b).
- Figure 10. Low weight hydrocarbon selectivity and olefin to alkane ratios in the presence and absence of pyridine.










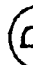
-  2-Way 3-Port Valve
-  2-Way 4-Port Valve
-  2-Way 6-Port Valve
-  4-Way 5-Port Valve
-  Metering Valve
-  Capillary Flow Resistance
-  Vent
-  Pressure Gauge

Figure 1

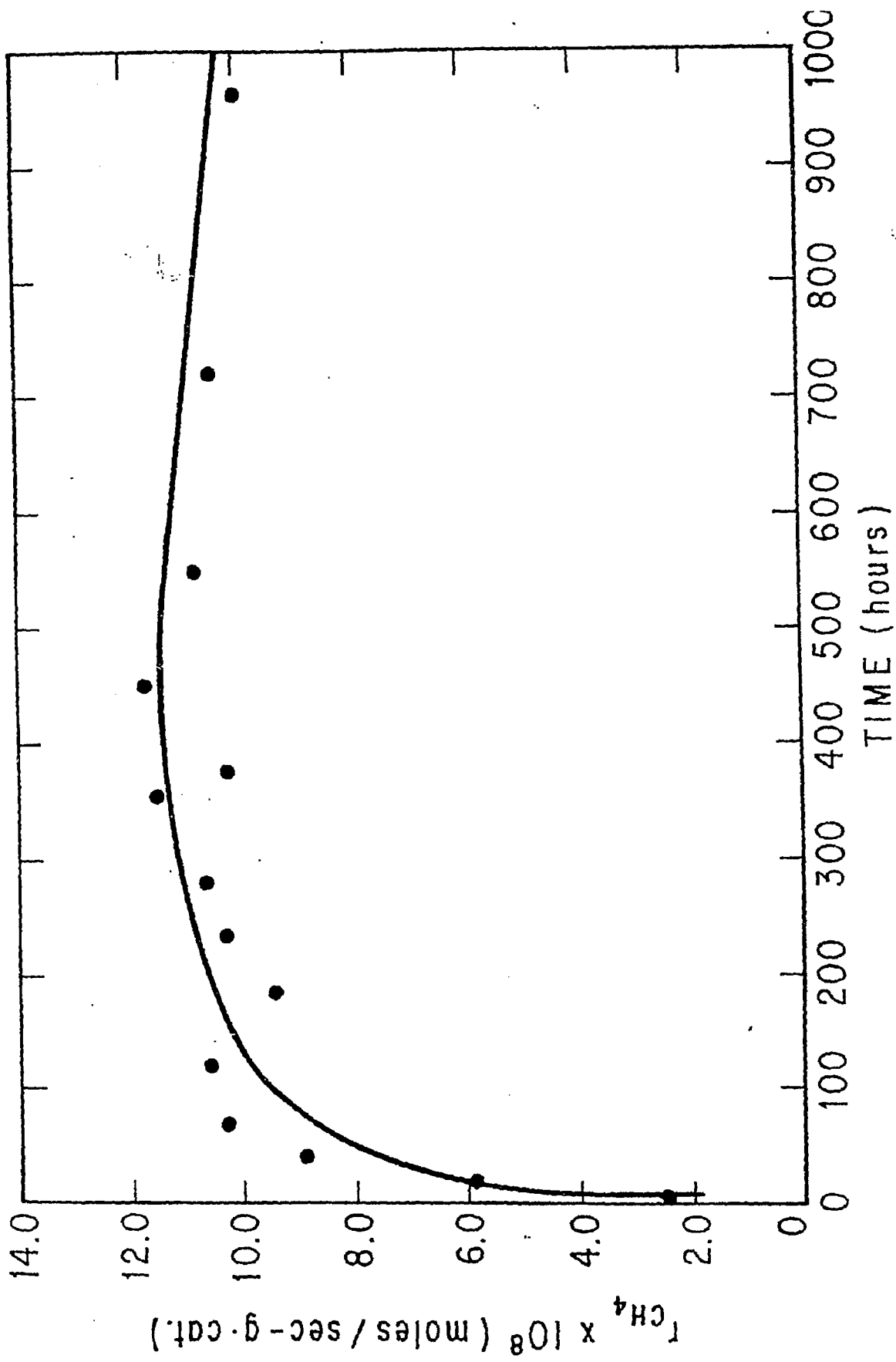


Figure 2

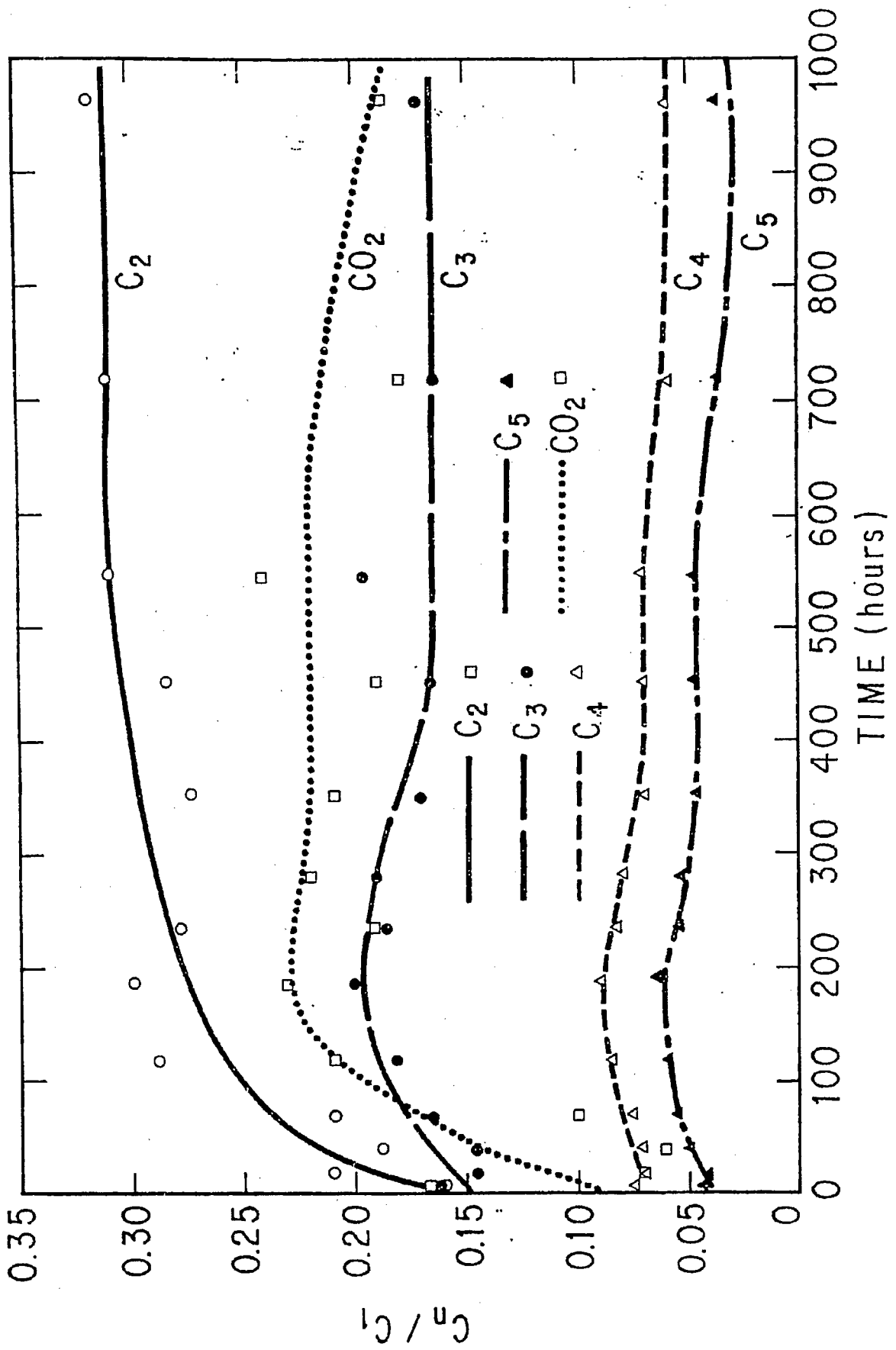


Figure 3

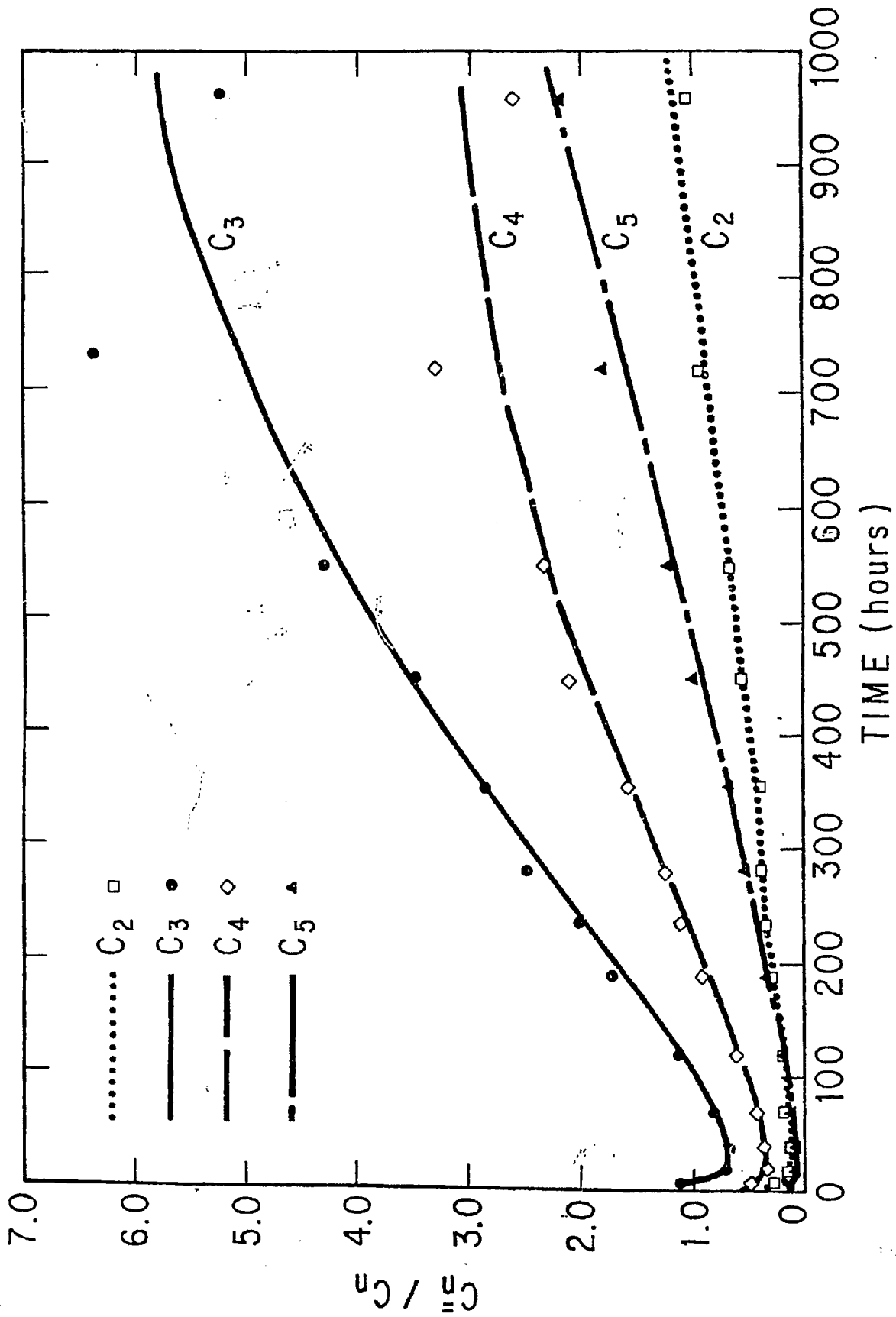


Figure 4

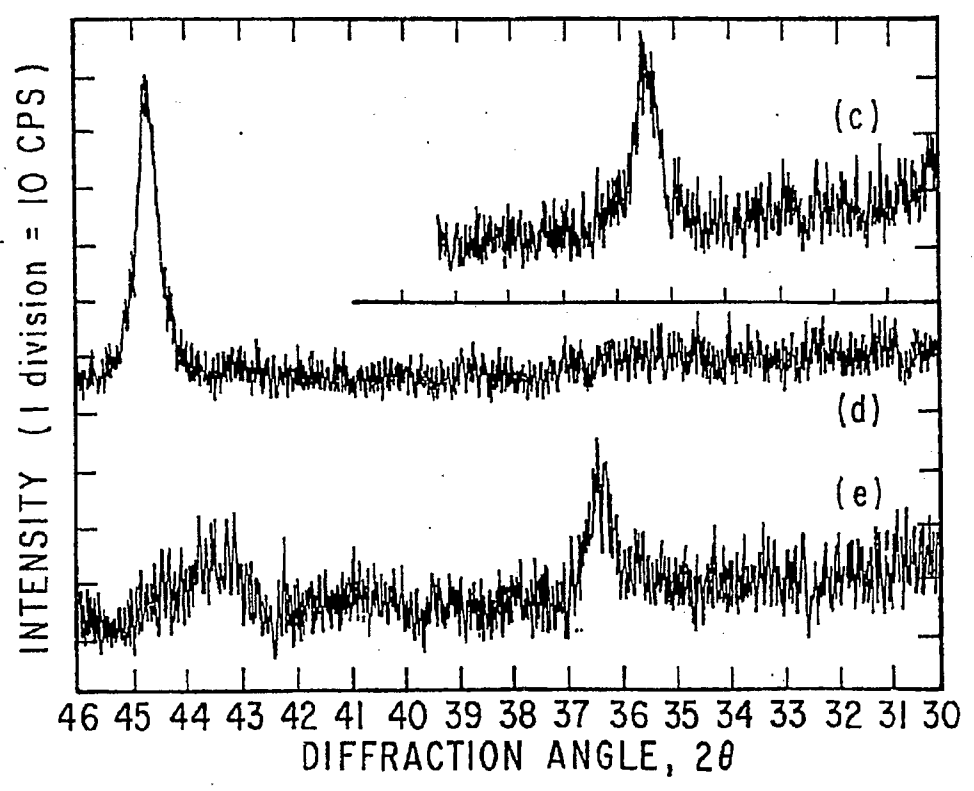
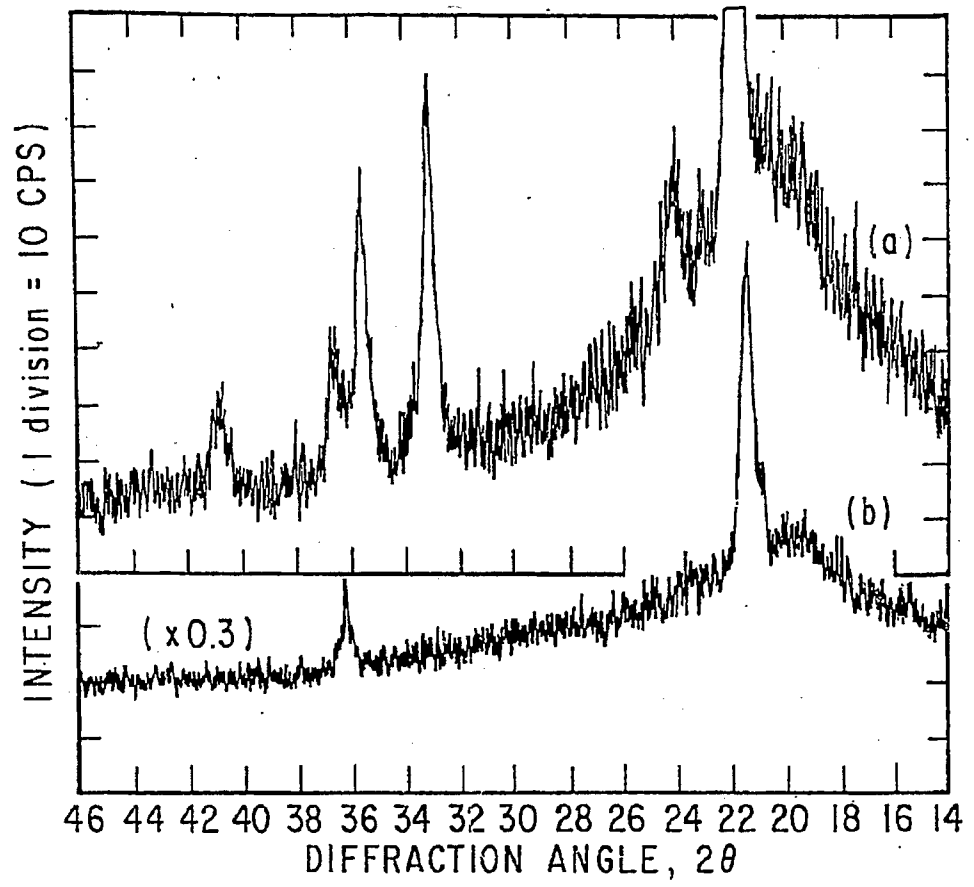


Figure 5

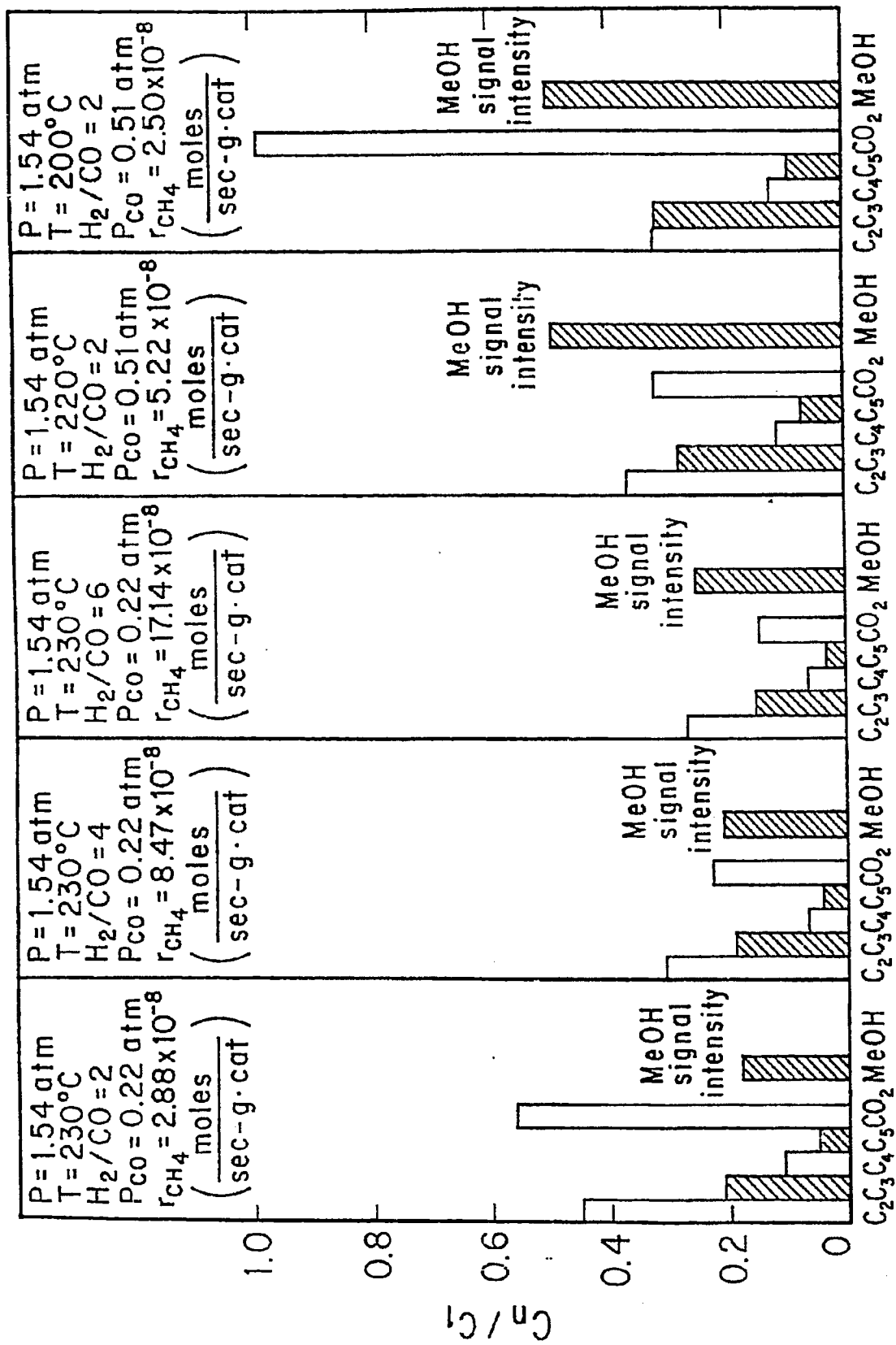


Figure 6

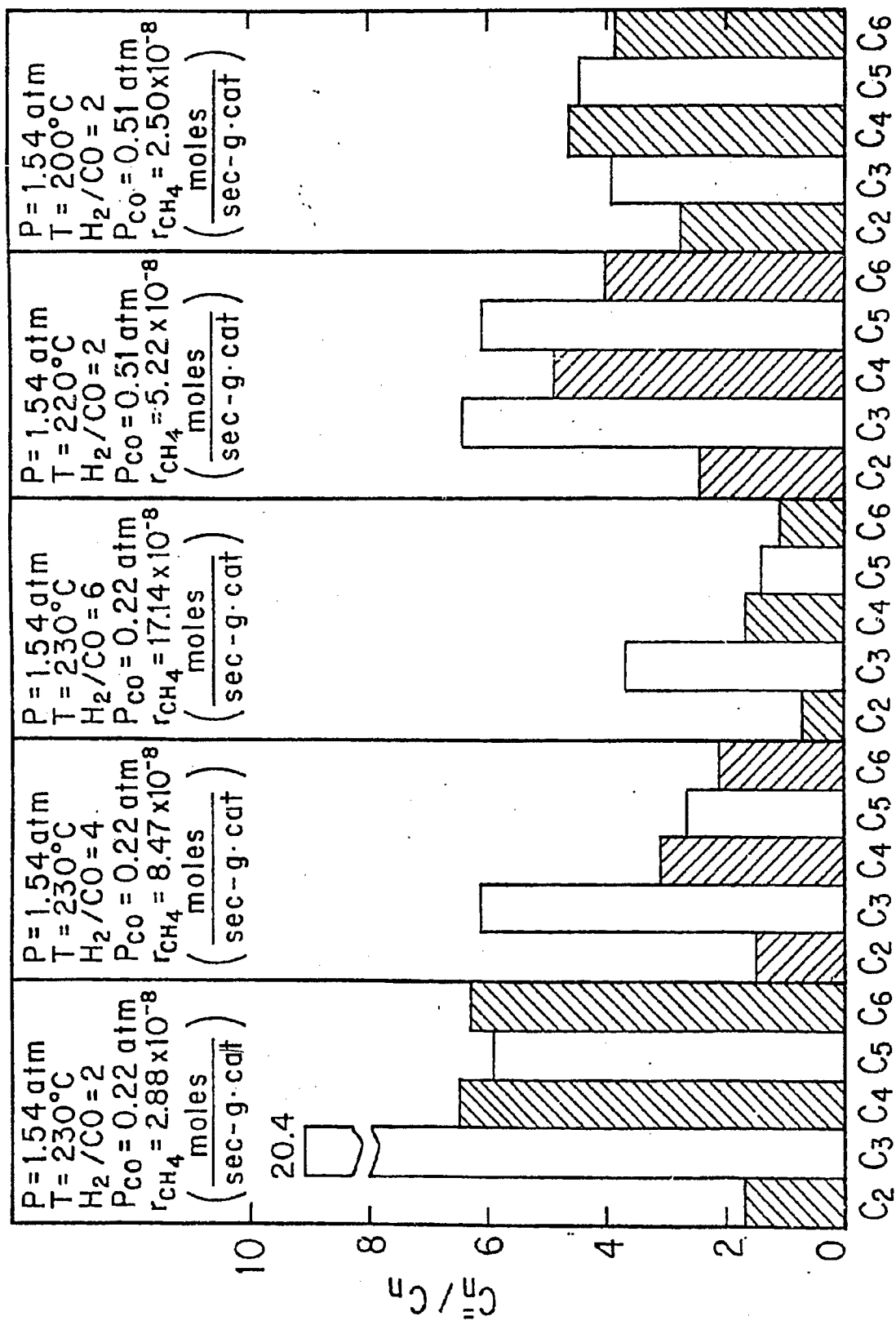


Figure 7

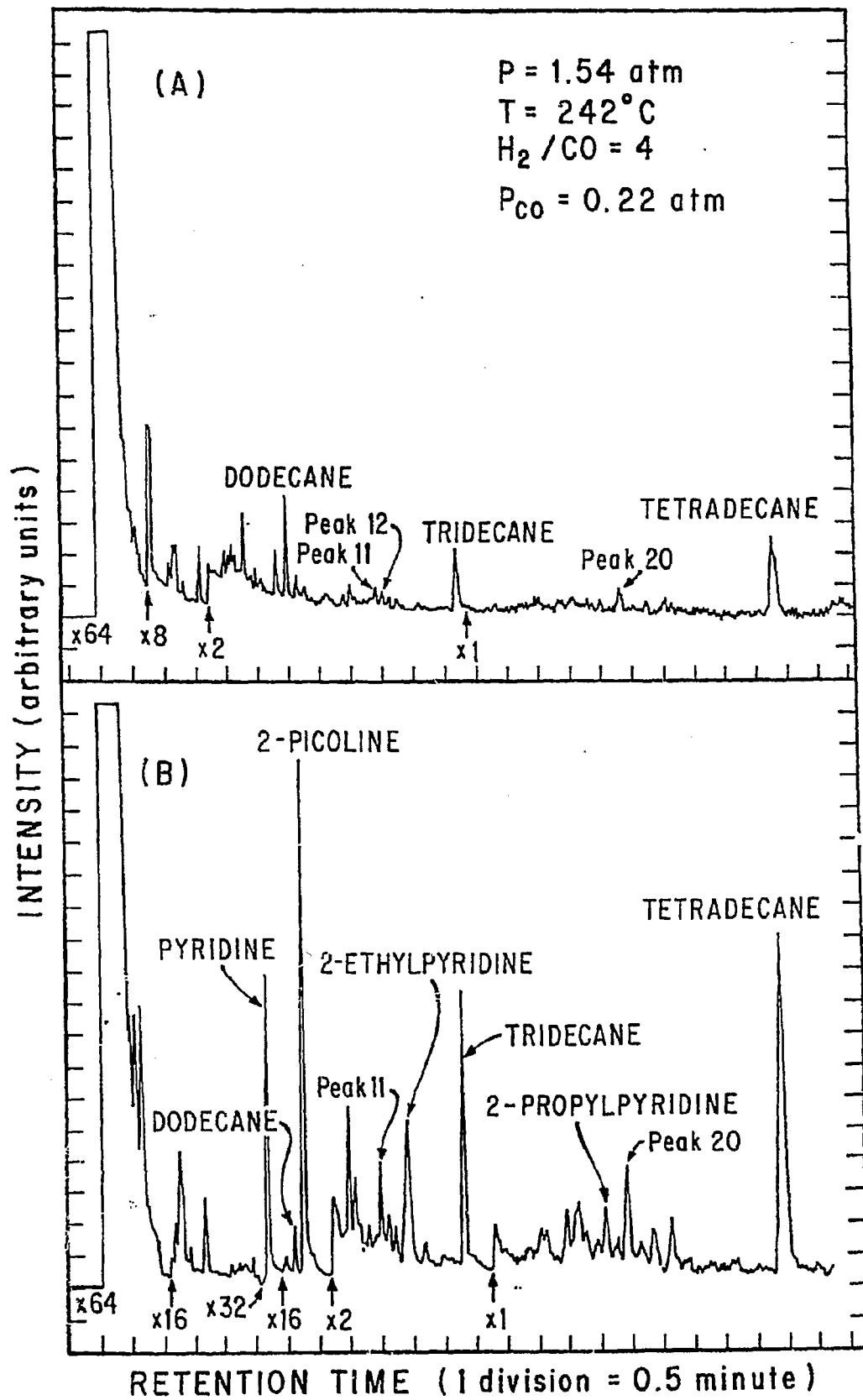


Figure 8

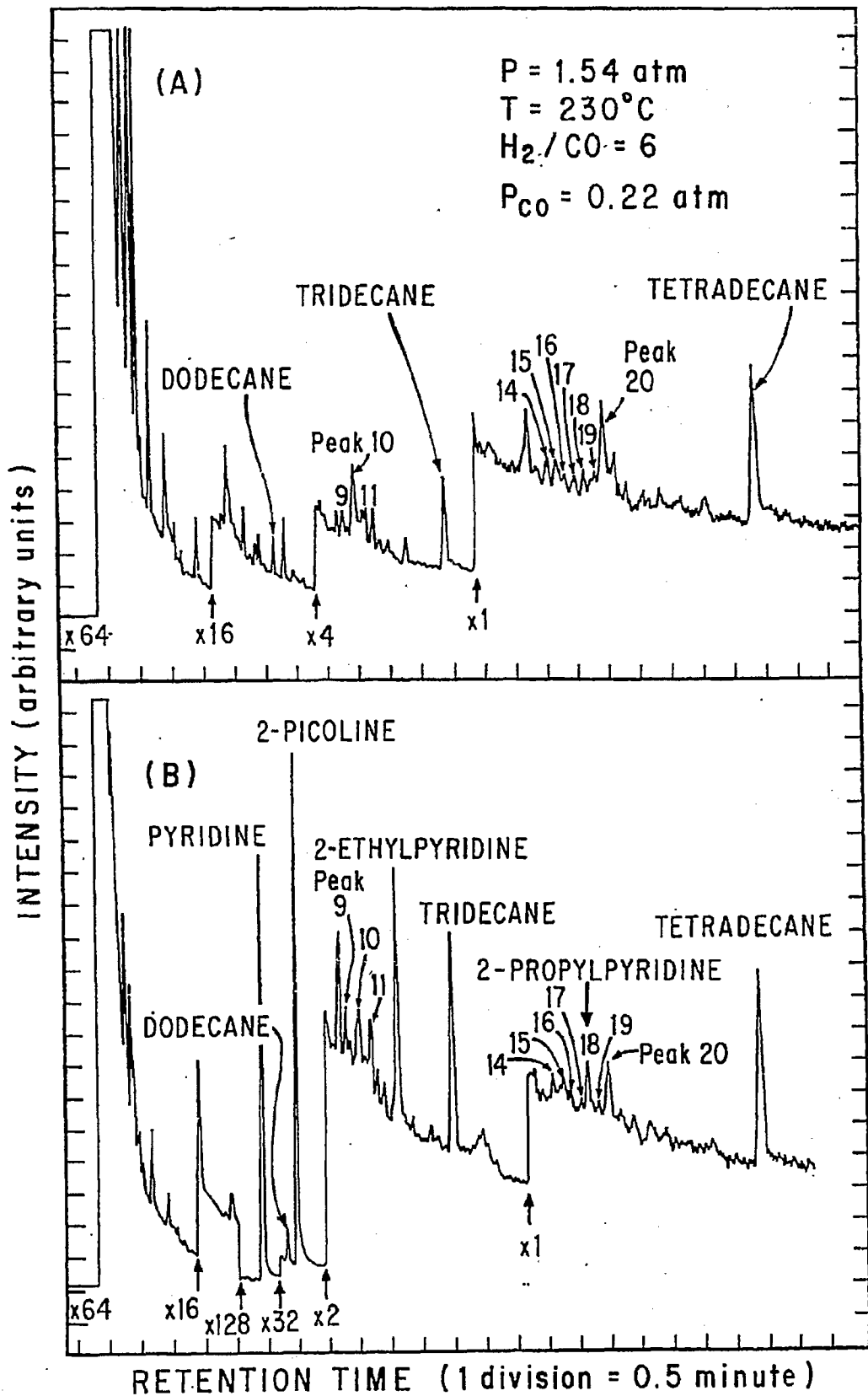


Figure 9

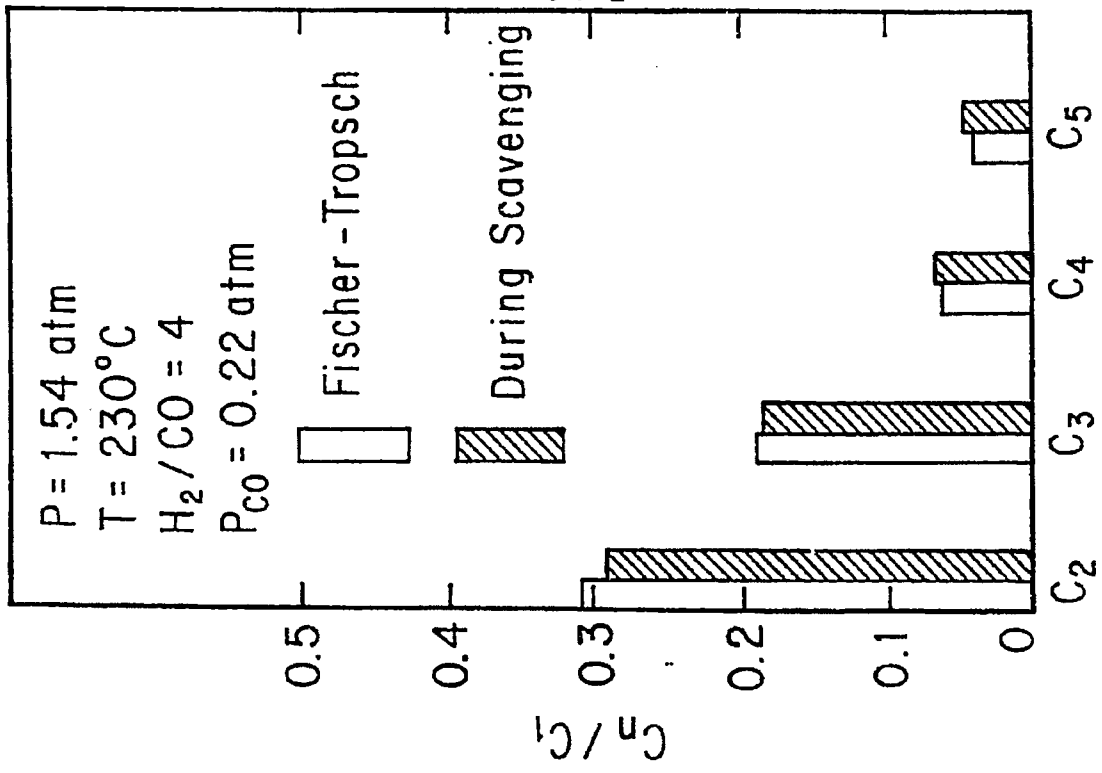
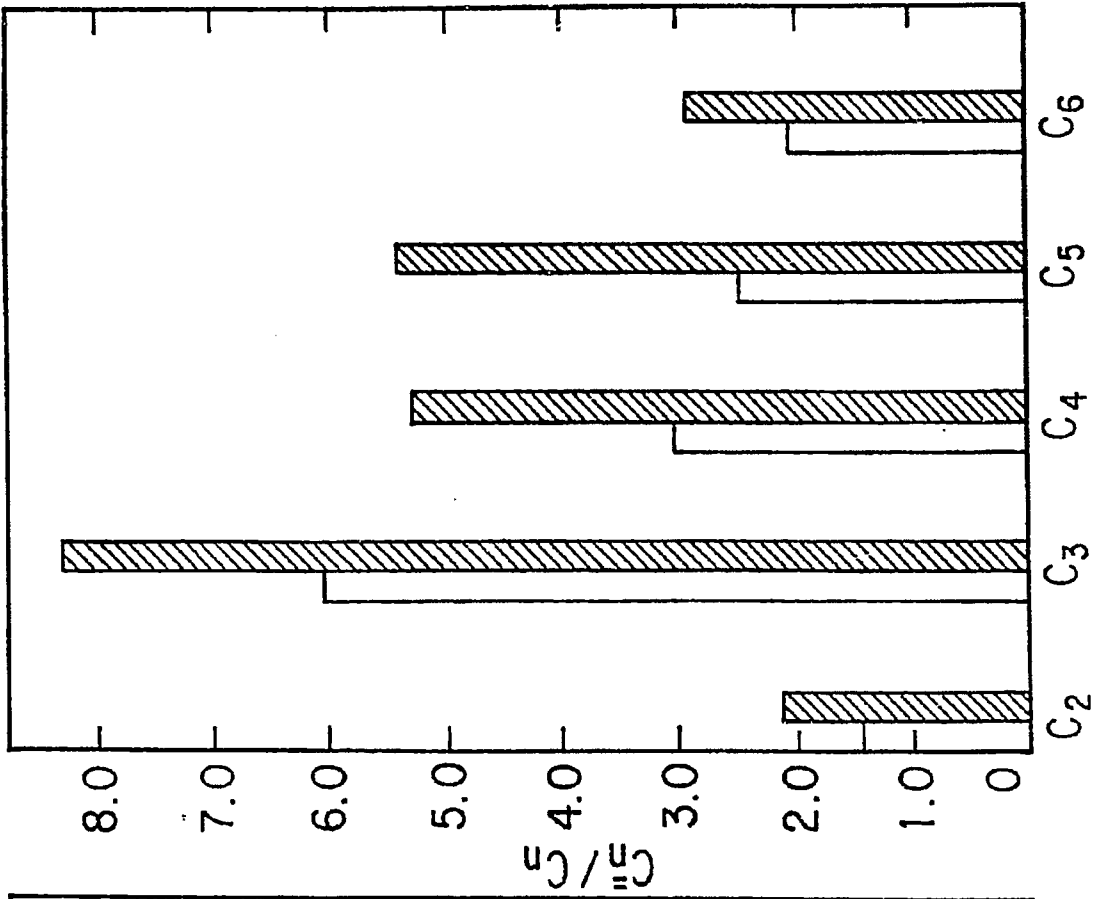


Figure 10